SEMARAK ILMU PUBLISHING

Journal of Advanced Research in Applied Sciences and Engineering Technology

Journal homepage:
https://semarakilmu.com.my/journals/index.php/applied_sciences_eng_tech/index
ISSN: 2462-1943

Comparison of Non-Linear Impedance AC Response of 10 and 20 Multiple Quantum Wells (MQWs) p-i-n Diode with DBR Towards Low Leakage Current Generation of Optoelectronic Device

Nur Fadzilah Basri[1,2], Afishah Alias[1,*], Megat Muhammad Ikhsan Megat Hasnan[3], Mohammad Syahmi Nordin[4], Fahrettin Sarcan[5], Khairul Anuar Mohamad[6]

[1] Department of Physics, Faculty of Applied Science and Technology, Universiti Tun Hussein Onn Malaysia, Pagoh Higher Education Hub, 84600 Muar, Johor, Malaysia
[2] Preparatory Centre for Science and Technology, Universiti Malaysia Sabah, 88400 Kota Kinabalu, Sabah, Malaysia
[3] Electric and Electronics Department, Faculty of Engineering, Universiti Malaysia Sabah, 88400 Kota Kinabalu, Sabah, Malaysia
[4] MT Data Driven Sdn. Bhd., Laurel Laman View, 63000 Cyberjaya, Selangor, Malaysia
[5] Nano and Optoelectronic Research Laboratories, Physics Department, Science Faculty, Istanbul University, 34134 Vezneciler, Istanbul, Turkey
[6] Microelectronic and Nanotechnology – Shamsuddin Research Centre (MiNT-SRC), Faculty of Electrical and Electronic Engineering, Universiti Tun Hussein Onn Malaysia, Parit Raja, 86400 Batu Pahat, Johor, Malaysia

ABSTRACT

This study explores the leakage current behaviour in multi-quantum well (MQW) devices using dielectric analysis. MQWs integrated with distributed Bragg reflector (DBR) show promise in enhancing optoelectronic device performance. Impedance spectroscopy and dark current-voltage measurements were conducted on 10 MQWs and 20 MQWs. The results indicate that 20 MQWs exhibit lower dielectric loss and leakage current compared to 10 MQWs. Understanding and minimizing resistive and polarization losses can improve the power efficiency and signal quality of optoelectronic devices. These findings demonstrate the importance of dielectric analysis for optimizing MQW-based optoelectronic devices.

Keywords:
Multi-quantum wells (MQWs); Leakage current; Impedance spectroscopy

1. Introduction

The integration of multi-quantum wells (MQWs) into a p-i-n diode configuration has emerged as a highly promising semiconductor device for diverse optoelectronic applications. The p-i-n structure, composed of p-type, intrinsic, and n-type semiconductor layers, synergistically combines with MQWs to augment the optical and electronic characteristics of the laser diodes [1,2], light-emitting diodes [3,4] and p-i-n infrared photodetector device [5-7].

To further optimize device performance, the incorporation of dilute nitride into the multi-quantum well (MQW) structure has been employed [8-10]. This enables precise tuning of the material's bandgap, facilitating the emission or detection of light at specific wavelengths [11-13]. Additionally, the integration of the MQW structure serves to enhance the optical properties of the

* *Corresponding author.*
E-mail address: afishah@uthm.edu.my

https://doi.org/10.37934/araset.XX.X.7686

device [14,15]. The utilization of distributed Bragg reflector (DBR) in MQW structures has proven advantageous in optimizing light-matter interactions, resulting in enhanced performance and efficiency of various optoelectronic devices based on quantum wells including lasers, photodetectors, and modulators [16,17]. DBR are composed of alternating layers of materials with different refractive indices that establish an optical cavity within the diode structure, enabling multiple reflections of light within the active region resulting in improved absorption or emission of photons. This is exemplified in the work of [1]Liu *et al*., [18] where a DBR was integrated with a strained GaAs/GaAsP superlattice photocathode, resulting in a record-level quantum efficiency. DBR was also found to provide substantial improvements in LED device performance whereas, in tuneable lasers, DBR was reported to enhance the output power, allowing for the attainment of a single-mode continuous wave output [19,20]. Additionally, DBR plays a crucial role in refining the colour purity of monolithic full-colour micro-LEDs by reflecting non-absorbed blue light towards the MQWs and increasing the probability of excitation and enhancing the colour output [21].

MQWs p-i-n diodes integrated with DBR exhibit unique nonlinear characteristics, requiring the utilization of complex mathematical models and nonlinear equivalent circuits for precise prediction and comprehension of their behaviour to effectively design and optimize the performance for a wide range of applications. Failure analysis is a widely utilized practice to evaluate the electrical performance of diodes and semiconductor devices. Various techniques are commonly employed within failure analysis, including the reverse bias method, I-V measurement [22], leakage current versus temperature method [23,24], time-dependent leakage current analysis [25], wafer-level testing [26], and high voltage testing. These methods collectively provide comprehensive insight into leakage current behaviour, ensuring optimal performance and suitability of p-i-n diodes for various applications.

This study initiates the investigation of Multiple Quantum Wells (MQWs) AC response to elucidate the leakage current behaviour in MQWs devices based using dielectric analysis. One must consider the non-linear I-V characteristics to determine dark leakage current. Understanding the non-linear nature of leakage current in non-linear devices is crucial for device characterization, design optimization, and ensuring proper functioning in various operating conditions. This study is the first for comparing the non-linear impedance AC response of 10 and 20 Multi-quantum Wells (MQWs) of p-i-n Diode with distributed Bragg reflector (DBR). The analysis of impedance spectra under different AC conditions provides valuable insights into the dielectric properties that play a significant role in reducing leakage current generation in optoelectronic devices.

2. Methodology

2.1 MQWs Device Preparation

The sample was developed on highly n-doped, (100)-oriented GaAs using the VG V80 Molecular Beam Epitaxy (MBE) system [16]. The dilute nitride samples were fabricated in a class J-10000 cleanroom facility at the University of Essex to ensure their purity. The preparation for electrical examination involved several procedures including cleaving, optical lithography, wet etching, and vacuum deposition. This research addressed two different samples, 10 MQWs and 20 MQWs respectively. The schematic representation of the utilized sample is depicted in Figure 1.

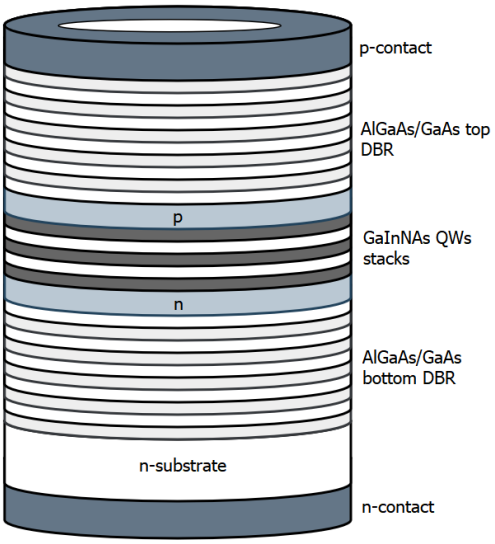

Fig. 1. Schematic diagram of MQWs p-i-n diode with DBR

2.2 Electrical Impedance Spectroscopy Measurement

Under dark conditions, electrical impedance spectroscopy (EIS) analysis was performed to investigate the electrical properties of 10 MQWs and 20 MQWs p-i-n diodes with DBR. Dielectric loss analysis was conducted using various AC voltage application at zero DC bias. Impedance measurements were carried out using the Solartron 1260 Frequency Response Analyzers (FRA) and SMaRT impedance measurement software. The EIS measurements were fixed at a frequency range of 1 MHz and 1 Hz with FRA DC coupling. This range offers a balance between time and frequency resolution while exploring quantum effects, such as confined charge carriers in quantum wells. For the EIS measurement, the AC voltage was tested from 0.1 V and 1 V for 10 MQWs and 20 MQWs, respectively. By employing small AC signals, the sensitivity of impedance measurements is significantly enhanced, making it possible to detect even minor changes in impedance which is particularly crucial when studying relaxation processes. The open-circuit voltage was obtained from the dark I-V measurement. All measurements were performed in the Faraday shield Lakeshore Model CPX Cryogenic Probe Station under vacuum conditions. To confirm the integrity of the obtained EIS data, the Nyquist plot obtained from the impedance analysis was fitted with Kramers-Kronig (K-K) analysis.

The loss tangent plots for the samples were determined using the ratio of the imaginary dielectric permittivity to the real dielectric permittivity, as described by Hasnan *et al*., [27] in the Eq. (1), Eq. (2) and Eq. (3) as follows:

$$\tan\delta = \frac{\varepsilon_i}{\varepsilon_r} \tag{1}$$

$$\varepsilon_r = \frac{Z_i}{\left(Z_r^{\,2} + Z_i^{\,2}\right)}\left(\frac{d}{\omega\varepsilon_0 A}\right), \varepsilon_i = \frac{Z_r}{\left(Z_r^{\,2} + Z_i^{\,2}\right)}\left(\frac{d}{\omega\varepsilon_0 A}\right) \tag{2}$$

where d is electrode distance, ω is angular frequency, A is electrode surface area, Z_r is real impedance and Z_i is imaginary impedance.

The relationship of dielectric loss with leakage current is directly proportional based on the governing Eq. (3) below where ε_0 is vacuum permittivity, ω is dielectric frequency relaxation in radian, E is electric field strength, and ε''_{total} is total imaginary parts of the complex permittivity respectively. Based on the governing equation, the total dark current density. The dielectric loss trend that obtained from impedance analysis will be correlated with the leakage current from the I-V characteristic.

$$J_{total} = \omega \varepsilon_0 \varepsilon''_{total} \tan \delta E \tag{3}$$

2.3 Current Density-Voltage (I–V) Measurement

For the dark current-voltage (I-V) measurement of the sample, this study employed a combination of the Lakeshore Model CPX Cryogenic Probe Station and the Keysight Agilent B1500A semiconductor device parameter analyser (SPA). The voltage sweep ranged from 0.5 to -2 V. The selected voltage range encompasses both forward and reverse bias conditions commonly applied to p-i-n diode, enabling the investigation on its behaviour across various bias levels. These measurements were conducted at room temperature.

3. Results

3.1 Impedance Spectroscopy Analysis

To characterize and analyse the dielectric loss in MQW devices, techniques such as electrical impedance spectroscopy (EIS) are commonly employed [28,29]. EIS measures the impedance response of the device at different frequencies, allowing the determination of parameters such as resistance, and dielectric loss [30]. In EIS Nyquist plots, the appearance of a semicircle shape is commonly observed which arises due to the presence of capacitive and/or inductive components in the impedance of the system. The semicircle shape in the Nyquist plot indicates a frequency-dependent behaviour in the system. At high frequencies, the impedance is dominated by resistive components, leading to a nearly flat portion of the semicircle close to the real axis. As the frequency decreases, capacitive and inductive components start to play a more significant role, causing the impedance to deviate from the real axis, forming the semicircle arc.

Figure 2 and Figure 3 shows the Nyquist plot of 10 MQWs while Figure 4 and Figure 5 shows the Nyquist plot of 20 MQWs, both exhibiting semicircle shapes characteristic. These Nyquist plot displaying the complex impedance of the p-i-n diode. The x-axis represents the real part of the impedance (Z'), which corresponds to the resistance, while the y-axis represents the imaginary part of the impedance (Z"), corresponding to the reactance. The plot provides valuable information about the electrical behaviour of the system at different frequencies. The trend of the semicircle for 10 MQWs shows same shape characteristics for all AC applied with changes of semicircles size as shown in Figure 2 and Figure 3.

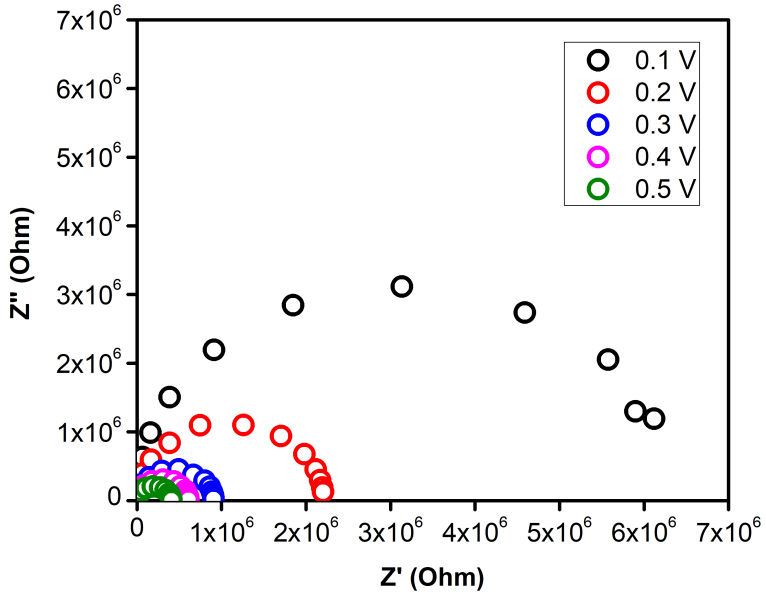

Fig. 2. Nyquist plot for 10 MQWs DBR at 0V DC bias at 0.1 V to 0.5 V AC applied

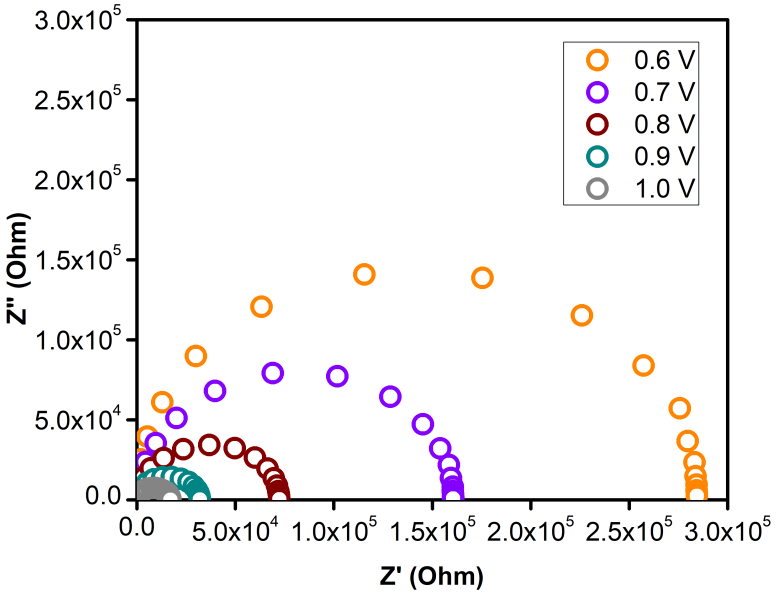

Fig. 3. Nyquist plot for 10 MQWs DBR at 0 V DC bias at 0.6 V to 1.0 V AC applied

In Nyquist plots, the appearance of small and large semicircles represents distinct electrical phenomena within the material. A small semicircle, characterized by a small radius, signifies a relatively fast relaxation process and few traps. Conversely, a large semicircle with a larger radius indicates a slow relaxation process and the presence of a significant number of traps. Analysing the size and characteristics of these semicircles provides valuable insights into charge carrier dynamics, conductivity, and interface effects of the p-i-n diode devices. 20 MQWs shows unique characteristic where after 0.1 V the semicircle shape is changing to distinct of two overlapping semicircles as shown in Figure 4 and Figure 5. This trend is significantly different than that semicircle trends of device 10 MQWs. Device with 20 MQWs is suggested to have distinct charge trap-tunnelling mechanisms to suppress leakage current compared to the 10 MQWs devices. The total size of the radius of semicircle for 20 MQWs also largely different than 10 MQWs by one order magnitude higher. Hence, device

that having more quantum wells shows higher total device resistance and expected to produce lower leakage current respectively than 10 MQWs.

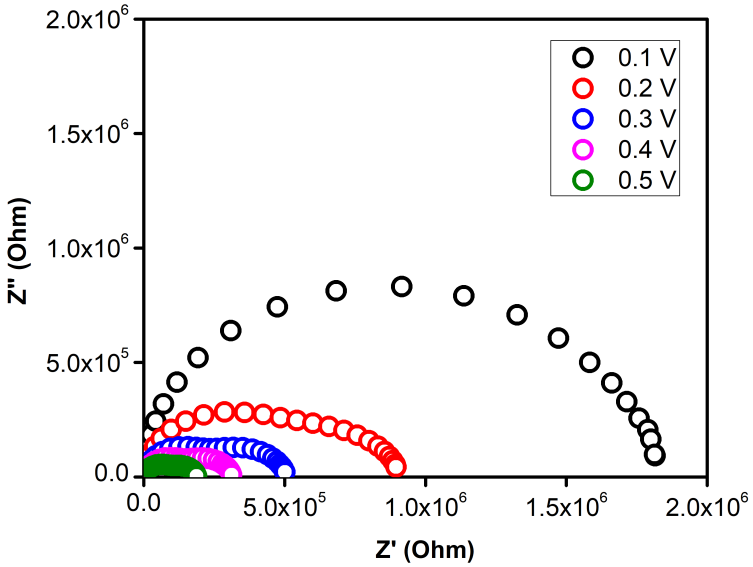

Fig. 4. Nyquist plot for 20QWs DBR at 0V DC bias at 0.1 V to 0.5 V AC applied

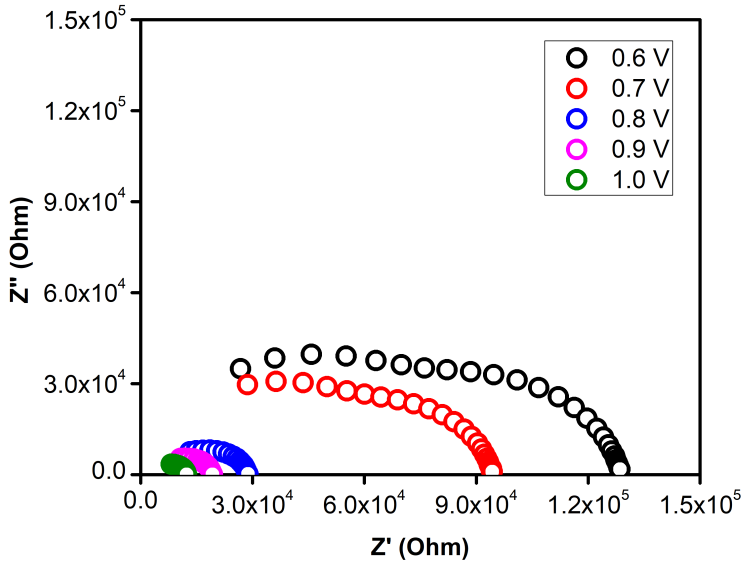

Fig. 5. Nyquist plot for 20QWs DBR at 0V DC bias at 0.6 V to 1.0 V AC applied

3.2 Dielectric Loss Tangent Analysis

Minimizing leakage current is crucial for achieving low-power operation and reducing power consumption in optoelectronic devices [31]. The specific design and optimization of MQWs, p-i-n diode structures, and DBR layers will impact the resulting leakage current characteristics. The dielectric loss in multi-quantum well (MQW) devices is an important electrical property that affects their leakage current performances govern in Eq. (2) above. Dielectric loss refers to the dissipation of electrical energy as heat due to the interaction between the electric field and the dielectric material within the MQW structure [32]. In an MQW device, multiple thin layers of different

semiconductor materials are stacked together as shown in Figure 1. These layers form a quantum well structure with well-defined energy levels. When an electric field is applied across the device, the carriers (electrons and holes) within the quantum wells are affected, leading to changes in their energy states and mobility [33,34].

Dielectric loss in MQW devices primarily arises from two sources: resistive losses and polarization losses [35,36]. Resistive losses occur due to the resistance of the materials used in the device structure [37]. This resistance leads to the conversion of electrical energy into heat, resulting in power dissipation. The magnitude of resistive losses depends on the conductivity of the materials employed. From the trend of dielectric loss in function frequency at various of AC voltage as shown in Figure 6 and Figure 7, the 10 and 20 MQWs shows distinct trend of dielectric loss relaxation. Both shows decrease of dielectric loss in function of frequency with an increase of AC voltage.

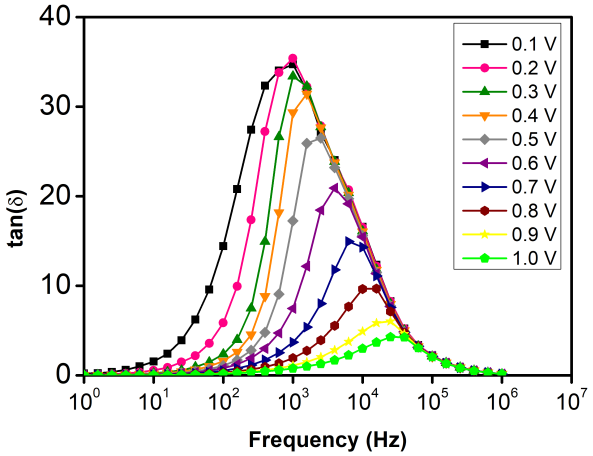

Fig. 6. Dielectric loss tangent for 10 MQWs DBR at 0 V DC bias at 0.1 to 1.0 V AC

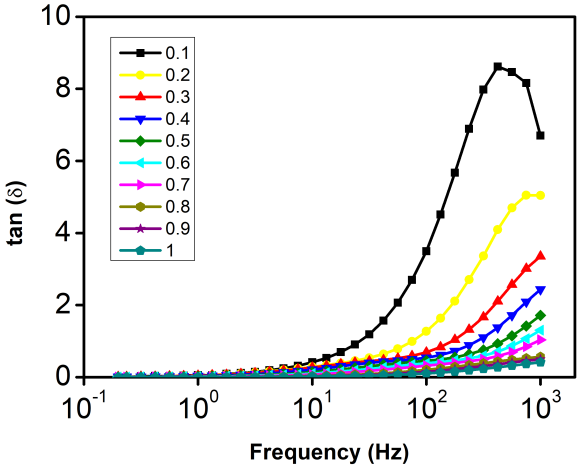

Fig. 7. Dielectric loss tangent for 20 MQWs DBR at 0 V DC bias at 0.1 to 1.0 V AC

To visualise the dielectric loss trend comparison of 10 MQWs and 20 MQWs clearly, the dielectric loss versus AC bias at 100 kHz from Figure 6 and Figure 7 is extracted and is replotted as shown in Figure 8. The figure shows very significant different of dielectric loss trend along the AC bias where the 20 MQWs is significantly lower than 10 MQWs. Polarization losses, on the other hand, are associated with the alignment of electric dipoles within the dielectric layers of the MQW device. When an electric field is applied, the dipoles undergo reorientation, and energy is dissipated as a

result. The magnitude of polarization losses is influenced by factors such as the dielectric constant of the materials, the frequency of the applied electric field, and the temperature.

Hence, the high resistance of semicircle total radius that observed from Nyquist plot in Figure 2, Figure 3, Figure 4, and Figure 5, indicating good correlation with the dielectric loss trend where high resistance of total device has suppressed the dielectric loss significantly by increasing the total of MQWs layer. Thus, from the dielectric observation, the leakage current of 20 MQWs is expected to produce lower dark leakage current than 10 MQWs and will be proven from the I-V characteristic in next section.

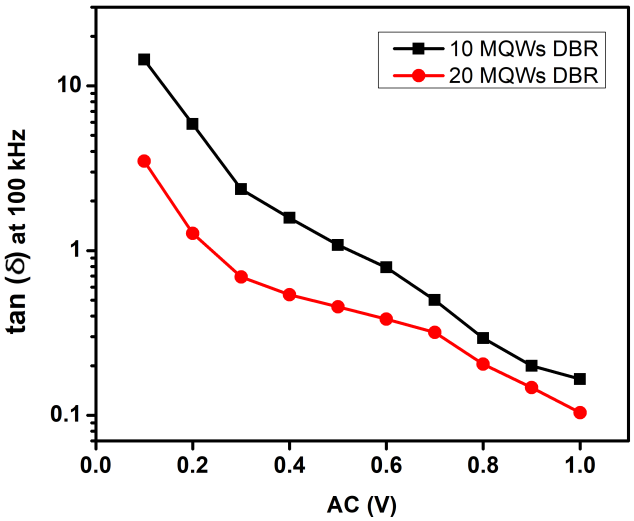

Fig. 8. Dielectric loss tangent for 10 MQWs and 20 MQWs DBR at 0V DC bias at 0.1 to 1.0 V AC

3.3 Dark Current-Voltage (I-V) Analysis for 10 MQWs and 20 MQWs

Figure 9 shows dark I-V characteristics for 10 and 20 MQWs. The trend shows good correlation with dielectric loss trend in Figure 8. The leakage current of the 20 MQWs is significantly lower than 10 MQWs by one order magnitude higher where the leakage current values for 10 MQWs and 20 MQWs are 1.57 $x10^{-8}$ Acm^{-2} and -2.7x 10^{-9} Acm^{-2} respectively. Understanding the dielectric loss in MQW devices in previous section shows crucial understanding for optimizing MQWs structure through dielectric loss performance. Minimizing resistive losses and dielectric losses thus is suggested to improve power efficiency, while reducing polarization losses that can enhance the optoelectronic device's response and signal quality.

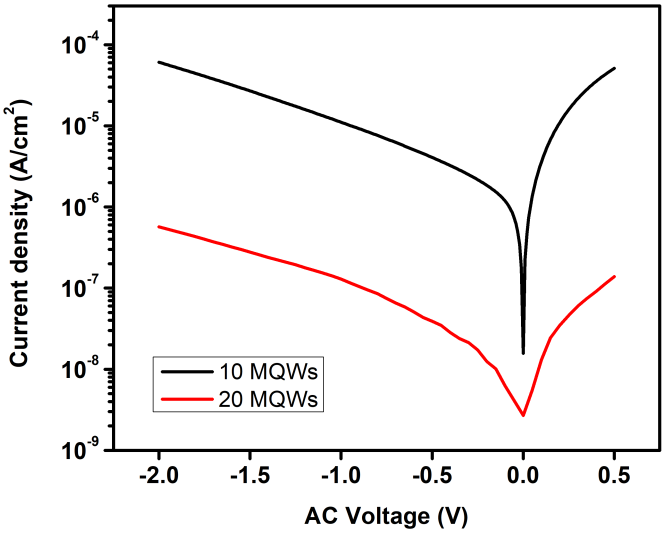

Fig. 9. Dark current-voltage measurements for 10 MQWs and 20 MQWs samples measured at T = 300 K

4. Conclusions

In conclusion, this study investigated the dielectric loss and leakage current behaviour of multi-quantum well (MQW) devices integrated with distributed Bragg reflector (DBR). The impedance spectroscopy analysis revealed distinct characteristics in the Nyquist plots of 10 MQWs and 20 MQWs, indicating differences in device resistance and charge trap-tunnelling mechanisms. Dielectric loss analysis demonstrated that 20 MQWs exhibited lower dielectric loss compared to 10 MQWs. The dark current-voltage (I-V) measurements further confirmed the superior performance of 20 MQWs with significantly lower leakage current. These findings highlight the significance of dielectric analysis in optimizing MQW-based optoelectronic devices for improved power efficiency and signal quality.

Acknowledgement

This research was supported by Universiti Tun Hussein Onn Malaysia through Tier1 Q159 and GPPS Q233. The authors would like to acknowledge Microelectronic and Nanotechnology – Shamsuddin Research Centre (MiNT-SRC), Universiti Tun Hussein Onn Malaysia for facilities and instruments provided throughout this research.

References

[1] Nash, G. R., S. J. B. Przeslak, S. J. Smith, G. De Valicourt, A. D. Andreev, P. J. Carrington, M. Yin *et al.,* "Midinfrared GaInSb/AlGaInSb quantum well laser diodes operating above 200 K." *Applied Physics Letters* 94, no. 9 (2009). https://doi.org/10.1063/1.3094879

[2] Guina, Mircea, Shu M. Wang, and Arto Aho. "Molecular Beam Epitaxy of Dilute Nitride Optoelectronic Devices." In *Molecular Beam Epitaxy*, pp. 73-94. Elsevier, 2018. https://doi.org/10.1016/B978-0-12-812136-8.00005-0

[3] Gu, Gil Ho, Dong Hyun Jang, Ki Bum Nam, and Chan Gyung Park. "Composition fluctuation of in and well-width fluctuation in InGaN/GaN multiple quantum wells in light-emitting diode devices." *Microscopy and microanalysis* 19, no. S5 (2013): 99-104. https://doi.org/10.1017/S1431927613012427

[4] Ching, Law Ruen, and Mohd Zulkifly Abdullah. "A Review of Moldflow and Finite Element Analysis Simulation of Chip Scale Packaging (CSP) for Light Emitting Diode (LED)." *Journal of Advanced Research in Fluid Mechanics and Thermal Sciences* 99, no. 1 (2022): 158-173. https://doi.org/10.37934/arfmts.99.1.158173

[5] Yahyaoui, N., N. Sfina, J. L. Lazzari, A. Bournel, and M. Said. "Performance evaluation of high-detectivity pin infrared photodetector based on compressively-strained Ge0. 964Sn0. 036/Ge multiple quantum wells by quantum modelling." *Semiconductor Science and Technology* 30, no. 8 (2015): 085016. https://doi.org/10.1088/0268-1242/30/8/085016

[6] Ghosh, Soumava, Anirban Bhattacharyya, Gopa Sen, and Bratati Mukhopadhyay. "Optimization of different structural parameters of GeSn/SiGeSn Quantum Well Infrared Photodetectors (QWIPs) for low dark current and high responsivity." *Journal of Computational Electronics* 20 (2021): 1224-1233. https://doi.org/10.1007/s10825-021-01668-w

[7] Jabarullah, Noor Hafidzah. "Temperature Dependence of Quantum Dots-in-well Infrared Photodetectors (QDIPs) Using Photoluminescence." *Journal of Advanced Research in Fluid Mechanics and Thermal Sciences* 54, no. 2 (2019): 133-141.

[8] Geng, Wei, Mathieu Manceau, Nancy Rahbany, Vincent Sallet, Massimo De Vittorio, Luigi Carbone, Quentin Glorieux, Alberto Bramati, and Christophe Couteau. "Localised excitation of a single photon source by a nanowaveguide." *Scientific reports* 6, no. 1 (2016): 19721. https://doi.org/10.1038/srep19721

[9] Baranowski, M., R. Kudrawiec, J. Misiewicz, and Mattias Hammar. "Nitrogen-related changes in exciton localization and dynamics in GaInNAs/GaAs quantum wells grown by metalorganic vapor phase epitaxy." *Applied Physics A* 118 (2015): 479-486. https://doi.org/10.1007/s00339-014-8794-4

[10] Xu, Lifang, Dinesh Patel, Carmen S. Menoni, Jeng-Ya Yeh, Luke J. Mawst, and Nelson Tansu. "Experimental evidence of the impact of nitrogen on carrier capture and escape times in InGaAsN/GaAs single quantum well." *IEEE Photonics Journal* 4, no. 6 (2012): 2262-2271. https://doi.org/10.1109/JPHOT.2012.2230251

[11] Richards, Robert D., T. B. O. Rockett, M. R. M. Nawawi, F. Harun, A. Mellor, T. Wilson, C. Christou, S. Chen, and J. P. R. David. "Light-biased IV characteristics of a GaAsBi/GaAs multiple quantum well pin diode at low temperature." *Semiconductor Science and Technology* 33, no. 9 (2018): 094008. https://doi.org/10.1088/1361-6641/aad72a

[12] Pareek, P., M. K. Das, and S. Kumar. "Numerical analysis of SiGeSn/GeSn interband quantum well infrared photodetector." *Opto-Electronics Review* 26, no. 2 (2018): 149-157. https://doi.org/10.1016/j.opelre.2018.03.002

[13] Pareek, Prakash, Mukul K. Das, and S. Kumar. "Responsivity calculation of group IV-based interband MQWIP." *Journal of Computational Electronics* 17 (2018): 319-328. https://doi.org/10.1007/s10825-017-1071-y

[14] Mohamad, Khairul Anuar, Mohammad Syahmi Nordin, Nafarizal Nayan, Afishah Alias, Abdul Rahman Mohmad, Adrian Boland-Thoms, and Anthony John Vickers. "Characterization of III-V dilute nitride based multi-quantum well pin diodes for next generation opto-electrical conversion devices." *Materials Today: Proceedings* 7 (2019): 625-631. https://doi.org/10.1016/j.matpr.2018.12.053

[15] Yanwachirakul, Warakorn, Naoya Miyashita, Hassanet Sodabanlu, Kentaroh Watanabe, Masakazu Sugiyama, Yoshitaka Okada, and Yoshiaki Nakano. "Carrier collection improvement in InGaAs/GaAsN multiple quantum well solar cell with flat conduction band." In *2018 IEEE 7th World Conference on Photovoltaic Energy Conversion (WCPEC)(A Joint Conference of 45th IEEE PVSC, 28th PVSEC & 34th EU PVSEC)*, pp. 1874-1877. IEEE, 2018. https://doi.org/10.1109/PVSC.2018.8548083

[16] Nordin, M. S., Fahrettin Sarcan, M. Gunes, A. Boland-Thoms, Ayşe Erol, and A. J. Vickers. "Temporal response of dilute nitride multi-quantum-well vertical cavity enhanced photodetector." *Journal of Electronic Materials* 47 (2018): 655-661. https://doi.org/10.1007/s11664-017-5815-z

[17] Chaqmaqchee, F. A. I., S. Mazzucato, Y. Sun, Naci Balkan, E. Tiras, M. Hugues, and M. Hopkinson. "Electrical characterisation of p-doped distributed Bragg reflectors in electrically pumped GaInNAs VCSOAs for 1.3 μm operation." *Materials Science and Engineering: B* 177, no. 10 (2012): 739-743. https://doi.org/10.1016/j.mseb.2011.12.035

[18] Liu, Wei, Yiqiao Chen, Wentao Lu, Aaron Moy, Matthew Poelker, Marcy Stutzman, and Shukui Zhang. "Record-level quantum efficiency from a high polarization strained GaAs/GaAsP superlattice photocathode with distributed Bragg reflector." *Applied Physics Letters* 109, no. 25 (2016). https://doi.org/10.1063/1.4972180

[19] Damilano, Benjamin, Stéphane Brochen, Julien Brault, Tasnia Hossain, François Réveret, Eric Frayssinet, Sébastien Chenot, Aimeric Courville, Yvon Cordier, and Fabrice Semond. "Growth of nitride-based light emitting diodes with a high-reflectivity distributed Bragg reflector on mesa-patterned silicon substrate." *physica status solidi (a)* 212, no. 10 (2015): 2297-2301. https://doi.org/10.1002/pssa.201532303

[20] Kanai, Takuya, Naoki Fujiwara, Yoshitaka Ohiso, Hiroyuki Ishii, Makoto Shimokozono, and Mikitaka Itoh. "2-μm wavelength tunable distributed Bragg reflector laser." *IEICE Electronics Express* 13, no. 16 (2016): 20160655-20160655. https://doi.org/10.1587/elex.13.20160655

[21] Chu, Shao-Yu, Hung-Yu Wang, Ching-Ting Lee, Hsin-Ying Lee, Kai-Ling Laing, Wei-Hung Kuo, Yen-Hsiang Fang, and Chien-Chung Lin. "Improved color purity of monolithic full color micro-LEDs using distributed Bragg reflector and blue light absorption material." *Coatings* 10, no. 5 (2020): 436. https://doi.org/10.3390/coatings10050436

[22] Ishimoto, Seiji, Dong-Pyo Han, Kengo Yamamoto, Ryoya Mano, Satoshi Kamiyama, Tetsuya Takeuchi, Motoaki Iwaya, and Isamu Akasaki. "Enhanced device performance of GaInN-based green light-emitting diode with sputtered AlN buffer layer." *Applied Sciences* 9, no. 4 (2019): 788. https://doi.org/10.3390/app9040788

[23] Larcher, Luca, Andrea Padovani, Francesco Maria Puglisi, and Paolo Pavan. "Extracting atomic defect properties from leakage current temperature dependence." *IEEE Transactions on Electron Devices* 65, no. 12 (2018): 5475-5480. https://doi.org/10.1109/TED.2018.2874513

[24] Hu, Lilei, Andreas Mandelis, Xinzheng Lan, Alexander Melnikov, Sjoerd Hoogland, and Edward H. Sargent. "Imbalanced charge carrier mobility and Schottky junction induced anomalous current-voltage characteristics of excitonic PbS colloidal quantum dot solar cells." *Solar Energy Materials and Solar Cells* 155 (2016): 155-165. https://doi.org/10.1016/j.solmat.2016.06.012

[25] Meyer, R., R. Liedtke, and R. Waser. "Oxygen vacancy migration and time-dependent leakage current behavior of Ba0. 3Sr0. 7TiO3 thin films." *Applied Physics Letters* 86, no. 11 (2005). https://doi.org/10.1063/1.1874313

[26] Gnanasegaran, Yogeswaran, Ahmad Anas Yusof, and Mohd Firdaus Shukri. "Study of Thermal-Fluid Analysis on Fusible Metal Bonding Application." *Journal of Advanced Research in Fluid Mechanics and Thermal Sciences* 62, no. 1 (2019): 88-102.

[27] Hasnan, MMI Megat, Norbani Abdullah, Suhana Mohd Said, MF Mohd Salleh, SA Mat Hussin, and N. Mohamed Shah. "Thermo-electrochemical generation capabilities of octahedral spin crossover complexes of Mn (II), Fe (II) and Co (II) with N-donor ligands and benzoate counter ion." *Electrochimica Acta* 261 (2018): 330-339. https://doi.org/10.1016/j.electacta.2017.12.145

[28] Oklobia, O., Soheil Komilian, and Torfeh Sadat-Shafai. "Impedance spectroscopy and capacitance–voltage measurements analysis: Impact of charge carrier lifetimes and mapping vertical segregation in bulk heterojunction P3HT: PCBM solar cells." *Organic Electronics* 61 (2018): 276-281. https://doi.org/10.1016/j.orgel.2018.06.003

[29] Nangia, Rakhi, Neeraj K. Shukla, and Ambika Sharma. "Impedance spectroscopy study of electrical properties of polymer blend interlayered Al/PEG-PVA/p-Si (MPS) structure." *Materials Research Express* 6, no. 9 (2019): 096315. https://doi.org/10.1088/2053-1591/ab33a3

[30] Pandey, Shukdev, Devendra Kumar, Om Parkash, and Lakshman Pandey. "Impedance spectroscopy: a powerful technique for study of electronic ceramics." In *Ceramic Materials-Synthesis, Characterization, Applications and Recycling*. IntechOpen, 2019. https://doi.org/10.5772/intechopen.81398

[31] Yoo, Changhyun, Jeesoo Chang, Sugil Park, Hyungyeong Kim, and Jongwook Jeon. "Optimization of gate-all-around device to achieve high performance and low power with low substrate leakage." *Nanomaterials* 12, no. 4 (2022): 591. https://doi.org/10.3390/nano12040591

[32] Fouad, S. S., G. B. Sakr, I. S. Yahia, D. M. Abdel-Basset, and F. Yakuphanoglu. "Capacitance and conductance characterization of nano-ZnGa2Te4/n-Si diode." *Materials Research Bulletin* 49 (2014): 369-383. https://doi.org/10.1016/j.materresbull.2013.08.065

[33] Kafafi, Zakya H., Raúl J. Martín-Palma, Ana F. Nogueira, Deirdre M. O'Carroll, Jeremy J. Pietron, Ifor DW Samuel, Franky So, Nelson Tansu, and Loucas Tsakalakos. "The role of photonics in energy." *Journal of photonics for energy* 5, no. 1 (2015): 050997-050997. https://doi.org/10.1117/1.JPE.5.050997

[34] Hasnan, MMI Megat, M. S. Nordin, N. Nayan, K. A. Mohamad, N. F. Basri, A. Alias, A. J. Vicker, and I. M. Noor. "Optoelectronic properties comparison of 10 and 20 multi quantum wells Ga0. 952In0. 048N0. 016As0. 984/GaAs pin photodetector for 1.0 μm wavelength." *Optical Materials* 127 (2022): 112272. https://doi.org/10.1016/j.optmat.2022.112272

[35] Demirezen, S., A. Kaya, S. Altındal Yerişkin, M. Balbaşı, and I. Uslu. "Frequency and voltage dependent profile of dielectric properties, electric modulus and ac electrical conductivity in the PrBaCoO nanofiber capacitors." *Results in physics* 6 (2016): 180-185. https://doi.org/10.1016/j.rinp.2016.03.003

[36] Tukiainen, A., A. Aho, V. Polojärvi, R. Ahorinta, and M. Guina. "High efficiency dilute nitride solar cells: Simulations meet experiments." *Journal of Green Engineering* 5, no. 3–4 (2016): 113-132. https://doi.org/10.13052/jge1904-4720.5348

[37] Bryant, Daniel, Peter Greenwood, Joel Troughton, Maarten Wijdekop, Mathew Carnie, Matthew Davies, Konrad Wojciechowski, Henry J. Snaith, Trystan Watson, and David Worsley. "A transparent conductive adhesive laminate electrode for high-efficiency organic-inorganic lead halide perovskite solar cells." *Advanced Materials* 26, no. 44 (2014): 7499-7504. https://doi.org/10.1002/adma.201403939